fractal and fractional

MDPI

Article

Finite-Time Stabilization of Unstable Orbits in the Fractional Difference Logistic Map

Ernestas Uzdila, Inga Telksniene, Tadas Telksnys, Minvydas Ragulskis *

Department of Mathematical Modelling, Kaunas University of Technology, Studentu 50-147, LT-51368 Kaunas, Lithuania; ernestas.uzdila@ktu.edu (E.U.); inga.telksniene@ktu.lt (I.T.); tadas.telksnys@ktu.lt (T.T.)

* Correspondence: minvydas.ragulskis@ktu.lt; Tel.: +370-698-22456

Abstract: A control scheme for finite-time stabilization of unstable orbits of the fractional difference logistic map is proposed in this paper. The presented technique is based on isolated perturbation impulses used to correct the evolution of the map's trajectory after it deviates too far from the neighborhood of the unstable orbit, and does not require any feedback control loops. The magnitude of the control impulses is determined by means of H-rank algorithm, which helps to reveal the pseudo-manifold of non-asymptotic convergence of the fractional difference logistic map. Numerical experiments are used to illustrate the effectiveness and the feasibility of the proposed approach, which is applicable beyond the studied fractional difference logistic map.

Keywords: fractional difference logistic map; impulse control; fractional derivative; unstable orbit

check for updates

Citation: Uzdila, E.; Telksniene, I.; Telksnys, T.; Ragulskis, M. Finite-Time Stabilization of Unstable Orbits in the Fractional Difference Logistic Map . *Fractal Fract.* **2023**, *7*, 570. https://doi.org/10.3390/fractalfract7080570

Academic Editor: Ivanka Stamova

Received: 3 May 2023
Revised: 9 July 2023
Accepted: 20 July 2023
Published: 25 July 2023

1. Introduction

The problem of controlling nonlinear discrete-time iterative maps is an active area of research in control theory, as such maps are applied in a plethora of fields including engineering, physics, biomedicine, population dynamics and economics [1,2].

A survey of classical control problems and schemes for nonlinear iterative maps is given in [3], while some more recent examples are given below. A neural-network based feedback control scheme for DC motors is proposed in [4]. The control of a predator–prey system with the Allee effect is realized via hybrid methods in [5]. A dynamic extended delayed feedback scheme for the control of the Rössler system is proposed in [6]. The Ott–Grebogi–York method is used to construct a computational chaos control scheme for the logistic map in [7]. Evolutionary metaheuristic methods are employed in the stabilization of the Hénon map in [8]. It is shown in [9] that model discovery methods for producing accurate and parsimonious parameter-dependent Poincaré mappings help to stabilize chaotic processes, including the Hénon map and the Rössler system. A finite-time model-free adaptive control scheme based on the nonparametric dynamic realization of the unknown nonlinear system is proposed in [10].

Fractional iterative maps form an important subset of discrete systems. Unlike their integer-order counterparts, such maps possess unique properties including non-locality and memory effects, which means that the state of the system is determined not only by its neighborhood, but globally, including a significant part (or, in some cases, all) past states [11]. Fractional maps find applications in a plethora of fields, such as image encryption [12,13], information security [14], epidemiology [15,16], economics [17], physics [18] and demographics [19].

Due to the wide range of applications, control of fractional iterative maps is a subject of many studies. A feedback control scheme for the fractional difference logistic map based on permutation entropy and fuzzy logic is constructed in [20]. Necessary optimality conditions of uncertain discrete-time fractional-order systems governed by difference equations are

derived in [21]. A backstepping method for the control of fractional single-input single-output systems is constructed in [22]. Containment control is successfully applied to discrete-time fractional-order multi-agent systems with a time delay in [23].

The main objective of this paper is to propose an impulse control scheme for the stabilization of unstable period-1 orbits of the fractional difference logistic map (which will be referred to as the fractional logistic map) [24,25]:

$$x_{n+1} = x_0 + \sum_{j=1}^{n+1} G_{j-1}^{\alpha}\left(a x_{n-j+1}\left(1 - x_{n-j+1}\right) - x_{n-j+1}\right), \quad j = 0, 1, \ldots, \tag{1}$$

where $G_0^{\alpha} = 1, G_j^{\alpha} = \left(1 - \frac{1-\alpha}{j}\right) G_{j-1}^{\alpha}, j = 1, 2, \ldots$. The parameter $\alpha \in (0, 1]$ describes the fractionality of (1): setting $\alpha = 1$ results in the classical logistic map.

Note that fractional order models, including continuous and discrete systems, do not have periodic motion due to the memory effect [26,27]. However, some trajectories of discrete fractional maps may exhibit asymptotic periodicity after some number of iterations. Such trajectories are referred to in the remainder of the text as asymptotically periodic orbits. In particular, it is known that the fractional difference logistic map (1), which is the main subject of this study, does possess asymptotically periodic orbits [25].

Most control schemes use feedback, which involves continuously monitoring the output of a system and adjusting the input to maintain a desired response [28]. The scheme proposed in this paper is based not on feedback, but impulse control, which involves making a perturbation of the system of a specific size (called the impulse) at a specific time based on predetermined fitness criteria [29]. The proposed scheme is less invasive than feedback control, as the fractional logistic map itself is not altered and a small perturbation is sufficient to temporarily stabilize the system.

2. Preliminaries

2.1. H-Ranks and Algebraic Complexity

H-ranks provide a straightforward but effective way to measure the algebraic complexity of a sequence. This measure has been successfully employed to analyze complexity in a number of different maps such as the invertible logistic map [30], the bouncer map [31], the Gauss map [32], as well as the fractional logistic map [33].

Consider a discrete sequence $\left(x_j; j = 0, 1, \ldots\right)$. The Hankel transform of this sequence is the sequence $\left(d_j; j = 1, \ldots\right)$, where d_j is the determinant of a jth order Hankel matrix H_j formed from $\left(x_j; j = 0, 1, \ldots\right)$:

$$d_j = \det\left(H_j\right), \; H_j = \begin{bmatrix} x_0 & x_1 & \ldots & x_{j-1} \\ x_1 & x_2 & \ldots & x_j \\ \vdots & \vdots & \ddots & \vdots \\ x_{j-1} & x_j & \ldots & x_{2j-2} \end{bmatrix}, \quad j = 1, 2, \ldots \tag{2}$$

If there is such $n \in \mathbb{N}$ that $d_n \neq 0$, but $d_{n+j} = 0, j = 1, 2, \ldots$, the sequence $\left(x_j; j = 0, 1, \ldots\right)$ represents a linear recurring sequence of order n [34].

The first n values determine these sequences completely, since the remaining elements can be computed via a linear recurrence relation. Furthermore, the computation of the order of a linear recurring sequence can be performed via the singular value decomposition (SVD). Consider a linear recurring sequence of order n and the corresponding Hankel matrix $H_{n+j}, j \geq 1$. The spectrum of H_{n+j} contains n nonzero eigenvalues and j zero eigenvalues, thus the singular values $\sigma_1^2 \geq \sigma_2^2 \geq \cdots \geq \sigma_{n+j}^2$ of matrix H_{n+j} are comprised of n nonzero elements and j zero-valued elements. Note that using this technique circumvents the need to compute the sequence $\left(d_j; j = 1, \ldots\right)$: it is sufficient to select a large enough N and compute the SVD of H_N.

The singular values $\sigma_j^2, j = 1, \ldots, N$ of matrix H_N are related to the eigenvalues λ_j, $j = 1, \ldots, N$ of H_N. In general, for any square matrix $A \in \mathbb{C}^{N \times N}$, the singular values are

the square roots of the non-zero eigenvalues of AA^* [35]. However, since H_N is real and symmetric, the singular values σ_j^2 are square roots of the eigenvalues of $H_N H_N^* = H_N^2$.

However, no real-world sequences can satisfy the linear recurrence condition both due to their more complex nature and the presence of noise. In this case, the H-rank of a sequence is computed using the following technique. Given a real-world (potentially noisy) sequence $(x_j; j = 0, 1, \dots)$, a threshold value ε and a Hankel matrix order N, the SVD of H_N is computed. The H-rank of sequence $(x_j; j = 0, 1, \dots)$ is equal to m, where m is the number of the singular value σ_m^2, $m \in \{1, \dots, N\}$ that satisfies the inequality

$$\sigma_m^2 > \varepsilon, \quad \sigma_{m+j}^2 \leq \varepsilon, \ j = 1, 2, \dots, N - m. \tag{3}$$

The selection of threshold ε and N is crucial: N has to be large enough to cover enough of sequence $(x_j; j = 0, 1, \dots)$ in order to evaluate its complexity, while ε has to be selected in such a way that the non-significant (close to zero) singular values would be disregarded [30]. The presented technique provides a way to measure the algebraic complexity of a sequence that is both easily understandable and effective to compute.

2.2. Classical Logistic Map and Types of Convergence

Despite its simplicity, the classical logistic map

$$x_{n+1} = a x_n (1 - x_n), \quad n = 0, 1, \dots \tag{4}$$

has been shown to possess surprisingly complex dynamics [36]. H-ranks have been shown to be an effective tool for the study of such dynamics, including the detection of convergence types. The bifurcation diagram of (4) and the plot of H-ranks is depicted in Figure 1. Note that the structure of the bifurcation diagram is fully contained within the plot of H-ranks. Moreover, intertwined manifolds of non-asymptotic convergence are also present in the pattern of H-ranks [30].

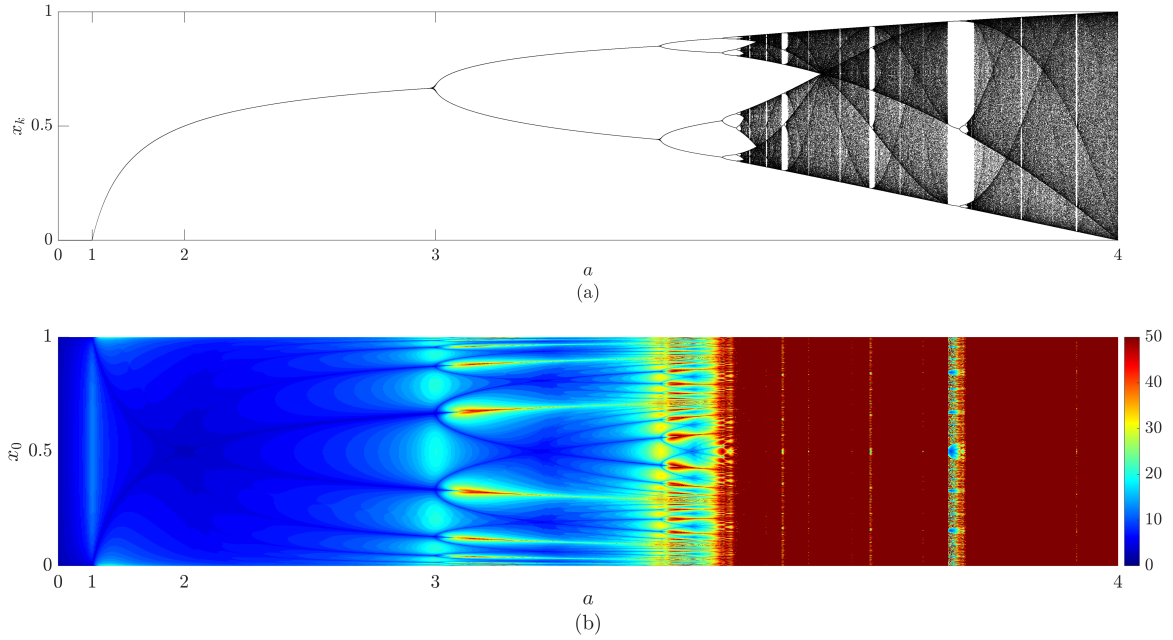

Figure 1. The bifurcation diagram of (4) is depicted in part (**a**); the plot of H-ranks is shown in part (**b**). Note that parameter values $N = 50$ and $\varepsilon = 10^{-10}$ were used for the computation of H-ranks.

Non-asymptotic convergence, as opposed to asymptotic convergence where the map converges to a fixed orbit as $n \to +\infty$, is a type of convergence for which the map enters a fixed orbit exactly after a finite number of iterations. This type of convergence can only

exist for non-invertible discrete maps (such maps where the value of $x_n = f^{-1}(x_{n+1})$ is not unique).

Classical logistic map can exhibit three types of convergence to a fixed point, which are illustrated in Figure 2 for a fixed value of parameter $a = 3.3$. Note that for this parameter value, two attractors exist: a stable period-2 attractor and an unstable period-1 attractor. Figure 2a depicts asymptotic convergence to a stable period-2 orbit. Selecting the initial condition, corresponding to the center of the low H-rank region, results in the non-asymptotic convergence to the stable period-2 orbit (Figure 2b). Finally, selecting the initial condition, corresponding to the center of the high H-rank region, results in the non-asymptotic convergence to the unstable period-1 orbit (Figure 2c).

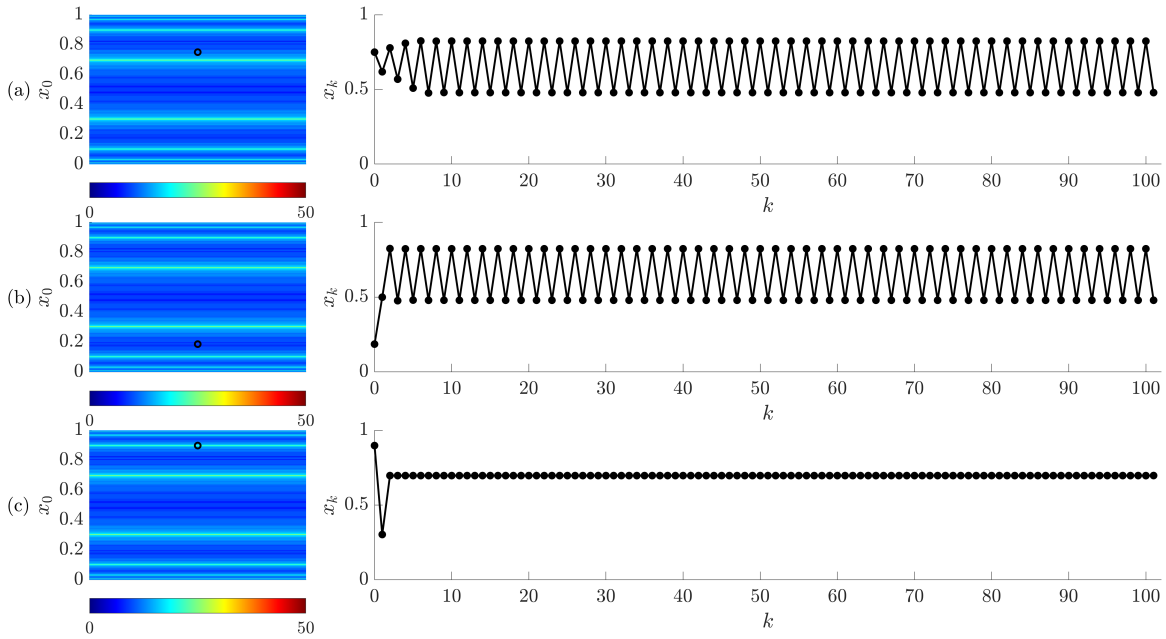

Figure 2. Three types of convergence processes to an orbit of a classical logistic map at $a = 3.3$. Parts (**a**–**c**) correspond to asymptotic convergence to the stable period-2 orbit, non-asymptotic convergence to the stable period-2 orbit, and non-asymptotic convergence to the unstable period-1 orbit respectively. Plots on the left side depict the values of H-ranks for $x_0 \in [0, 1]$ and $a = 3.3$. Plots on the right side illustrate the trajectories of the classical logistic map started from different initial conditions marked by a black circle in the corresponding plots of H-ranks.

2.3. Fractional Logistic Map

An essential property of the fractional difference logistic map (1) is the memory effect. If $\alpha \neq 1$, the nth element x_n depends on all preceding elements $x_0, x_1, \ldots, x_{n-1}$. In other words, the memory horizon of the fractional difference logistic map does reach the initial condition (though the influence of "older" elements decays exponentially as can be observed from the weight coefficients $G_j^{\alpha}, j = 0, 1, \ldots$).

The bifurcation diagram and plot of H-ranks for (1) are depicted in Figure 3. Types of convergence of (1) have already been analyzed using H-ranks in [33]. The main goal of this paper is to go one step further by proposing a control scheme for the fractional counterpart of the logistic map (1) based on the H-rank algorithm.

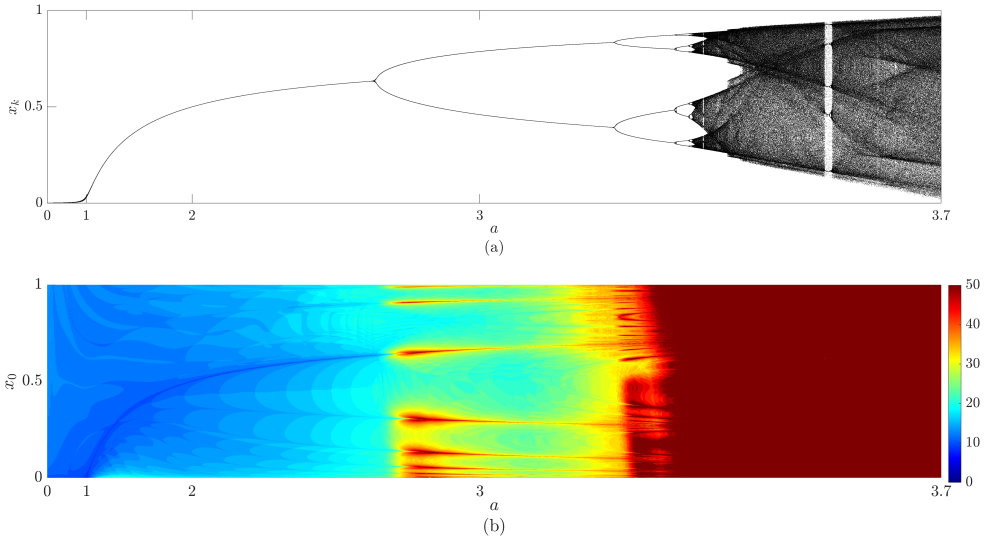

Figure 3. The bifurcation diagram of (1) for $\alpha = 0.8$ is depicted in part (**a**); the plot of H-ranks is shown in part (**b**). Parameter values $N = 50$ and $\varepsilon = 10^{-10}$ were used for the computation of H-ranks.

3. The Unstable Orbits of the Fractional Difference Logistic Map

The bifurcation diagram of the fractional difference logistic map (Figure 3) shows that period-1 orbit is unstable at $a = 3$. It is demonstrated in Figure 2c that the unstable period-1 orbit can be stabilized by choosing a proper initial condition of the classical logistic map. Therefore, before designing the scheme for the stabilization of unstable orbits, it is important to understand the behavior of the unstable period-1 orbit of the fractional difference logistic map.

In this section, we only address fixed points relevant to the construction of the impulse control scheme. A more detailed discussion on types of fixed points in fractional order systems can be found in [37–39].

3.1. The Existence of the Unstable Period-1 Orbit at $a = 3$

The first iteration of the fractional difference logistic map (1) is equivalent to the classical logistic map: $x_1 = ax_0(1 - x_0)$. The non-trivial fixed point for the classical logistic map reads: $x^* = 1 - \frac{1}{a}$ [36]. Thus, setting $x_0 = x^*$ results in $x_1 = x^*$. By induction, the fractional difference logistic map (1) yields $x_j = x^*$ for all $j = 0, 1, \ldots$. Thus, the fractional difference logistic map continuously remains on the unstable period-1 orbit if only the initial condition is set to $x_0 = 1 - \frac{1}{a}$ at $a = 3$.

3.2. The Existence of the Non-Asymptotic Convergence to the Unstable Period-1 Orbit

It is demonstrated in Figure 2c that non-asymptotic convergence to the unstable period-1 orbit does exist for the classical logistic map. It is important to understand that the same does exist for the fractional difference logistic map.

The existence of the non-asymptotic convergence to the unstable period-1 fixed orbit x^* for the fractional difference logistic map (1) would mean that there exists an iteration number $k \in \mathbb{N}$ such that:

$$x_k \neq x^*, \quad \text{but} \quad x_{k+j} = x^*, j = 1, 2, \ldots \tag{5}$$

Consider the case $k = 0$. As before, note that $x_1 = ax_0(1 - x_0)$ and solving for x_0 yields two values: $x_0^{(1)} = x^*$ and $x_0^{(2)} = \frac{1}{a}$. The first solution does not represent the element of the trajectory representing the non-asymptotic convergence because condition (5) does not hold true. However, taking $x_0 = \frac{1}{a}$ leads to $x_1 = x^*$. However, the next elements do not stay at x^* due to the memory effect of the fractional difference logistic map. For example, the second element x_2 reads:

$$\begin{aligned} x_2 &= x_0 + G_0^{\alpha}(ax_1(1-x_1) - x_1) + G_1^{\alpha}(ax_0(1-x_0) - x_0) \\ &= \frac{1}{a} + G_0^{\alpha} \cdot 0 + G_1^{\alpha} x^* = \frac{1}{a} + G_1^{\alpha}\left(1 - \frac{1}{a}\right). \end{aligned} \tag{6}$$

Thus, $x_2 = x^*$ only for some specific value of α. Even if such a value is chosen, there remains no way to ensure the equality $x_3 = x^*$. Thus, non-asymptotic convergence does not exist for fractional difference logistic map for $k = 0$.

Since non-asymptotic convergence does not exist for $k = 0$, it also cannot exist for $k = 1, 2, \ldots$ because the last iteration would result in the case that has already been discussed.

The above derivations lead to an important conclusion. It is impossible to find such an initial condition in the fractional logistic map that would yield a trajectory that would continuously remain at the unstable orbit.

This fact is illustrated in Figure 4, where $\alpha = 0.8$ and $a = 3$. The threshold parameter of the H-rank algorithm is set to $\varepsilon = 10^{-10}$, the maximum H-rank (the dimension of the Hankel matrix) is set to $N = 50$.

The asymptotic convergence to the asymptotically stable period-2 orbit occurs when the initial condition x_0 does not coincide with any of the bright bands in the pattern of H-ranks (Figure 4a). As mentioned previously, the non-asymptotic convergence is not possible for the fractional difference logistic map. However, a short non-asymptotic process yields a finite-time stabilization of the unstable period-1 orbit when the initial condition x_0 is set right over the bright band in the pattern of H-ranks (Figure 4b). Note that such finite-time stabilization of unstable orbits of the fractional difference logistic map by choosing an appropriate initial condition is already discussed and investigated in [33].

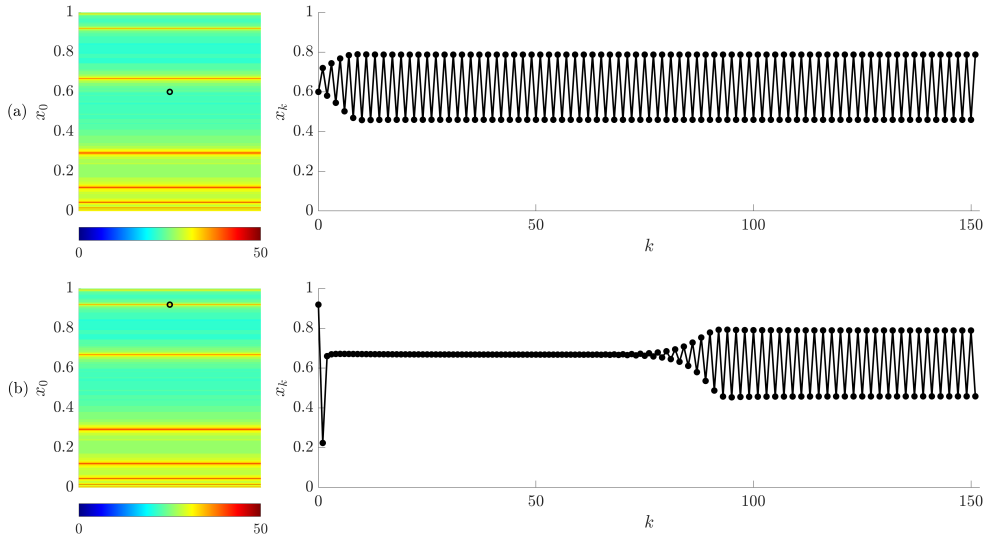

Figure 4. Types of convergence in the fractional logistic map for parameter values $\alpha = 0.8, a = 3$. Part (**a**) depicts asymptotic convergence to the period-2 asymptotically stable attractor. Part (**b**) temporary stabilization of the trajectory to the unstable period-1 attractor. Plots on the right represent trajectories of the fractional logistic map; plots on the left depict the H-ranks for initial conditions $x_0 \in (0, 1)$; the black circle indicates the initial condition from which the trajectories on the right begin. Note that in (**b**), the black circle is on the red band of high H-ranks.

4. The Memory Effects and the Naive Control Scheme

4.1. The Naive Control Scheme for the Classical Logistic Map

Let us consider the classical logistic map at $a > 3$ (after the first period doubling bifurcation). Then, the the period-1 orbit is unstable and the non-asymptotic convergence to the unstable period-1 orbit can be implemented by choosing a proper initial condition (Figure 2c).

However, let us consider a trajectory that does not converge non-asymptotically to the unstable period-1 orbit. For example, let us set the initial condition to $x_0 = x^* + \epsilon$, where $x^* = 1 - \frac{1}{a}$ ($a = 3.3$) and ϵ is the perturbation; $\epsilon \neq 0$. Such a trajectory $x_0, x_1, \ldots$ will converge to the stable period-2 orbit.

Let us assume that the objective of the control scheme is to bring back the trajectory to the unstable period-1 orbit when it travels from the point x^* further away than the threshold δ. In other words, the classical logistic map is iterated until an iteration m is found such that the following condition is satisfied:

$$|x_{m-1} - x^*| < \delta, \quad |x_m - x^*| \geq \delta, \tag{7}$$

The control scheme is straightforward. One needs to set $x_{m+1} = x^*$. It is clear that the classical logistic map will remain indefinitely in the unstable period-1 orbit. The magnitude of a discrete impulse required to stabilize the unstable period-1 orbit is equal to $|x_{m-1} - x^*|$. Such a control scheme is denoted as the naive control scheme for the classical logistic map.

4.2. The Naive Control Scheme for the Fractional Difference Logistic Map

Let us consider the naive control scheme for the fractional difference logistic map (1), as depicted in Figure 5. The black line in Figure 5b denotes the trajectory of the fractional logistic map before the control impulse; the gray line continues the same trajectory if no stabilization impulse is applied at iteration $k = 86$. The blue line represents the trajectory after the naive control impulse. It is clear that using this scheme does not result in neither finite-time nor continuous stabilization. Clearly, the stabilization of unstable orbits of the fractional difference logistic map requires a more complex approach.

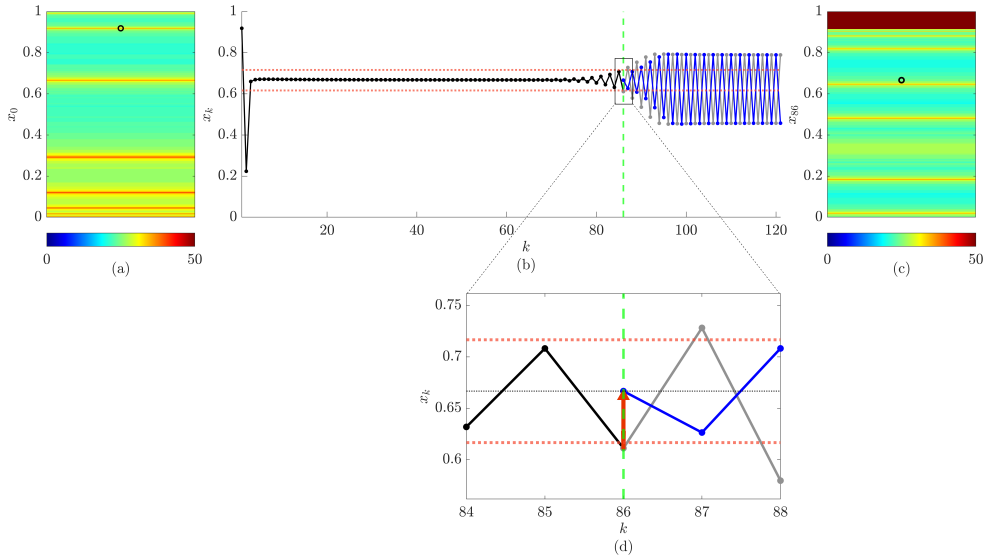

Figure 5. The naive stabilization scheme does not work for the fractional difference logistic map ($\alpha = 0.8, a = 3$, and the stabilization threshold $\delta = 0.05$). Part (**a**) depict H-ranks of fractional logistic map trajectories starting from the initial condition, where the black circle denotes the initial condition, chosen in such a way that the logistic map trajectory is temporarily stabilized. In part (**b**), fractional logistic map trajectories are depicted. Red dotted lines represent $x^* \pm \delta$; the green dashed line represents the iteration at which the stabilization is performed; the black line represents the initial part of the trajectory for which $|x_n - x^*| < \delta$ holds true; the gray solid line is the continuation of the black trajectory if no stabilization is performed; the blue line is the trajectory after performing naive stabilization by setting $x_{86} = x^*$. Part (**c**) depicts the H-ranks computed time-forward starting from the moment of stabilization, where the black circle denotes the position of the trajectory after the stabilization impulse x^*. Part (**d**) is a zoomed plot of the boxed area present in part (**b**), which details the stabilization process: when the initial trajectory intersects the red dotted line, the control impulse (red arrow) shifts the trajectory to x^*.

5. The Proposed Scheme Based on a Single Control Impulse

As shown in Figure 4b, there exist such initial conditions for which the trajectory of the fractional difference logistic map becomes stabilized around the period-1 orbit for a finite period of time. The proposed control scheme is constructed with the key idea about a control impulse, which must be used when the oscillations of the trajectory around the unstable orbit become unacceptably large. As demonstrated in Figure 5, a naive control strategy does not work for the fractional difference logistic map. Therefore, the feasibility of the control strategy based on a single control impulse does depend on the existence of such coordinates, which would yield transient processes capable to stabilize the unstable orbit (after it has started to diverge).

The apparent simplicity of the raised question is misleading. As noted previously, the nth element of the fractional difference logistic map depends on all preceding elements, including the initial condition. Changing a single coordinate of the trajectory at some iteration number k ($k > 0$) does not alter the past values of the trajectory at $k = 0, 1, ..., k-1$, and all the memory of the trajectory is taken into account. Note that if the control impulse is performed at iteration k, the value of $x_0, x_1, \ldots, x_k$ remains unchanged, as shown in Figure 5b,d. The impact of past iterations on the value of the fractional difference logistic map is depicted in Figure 6.

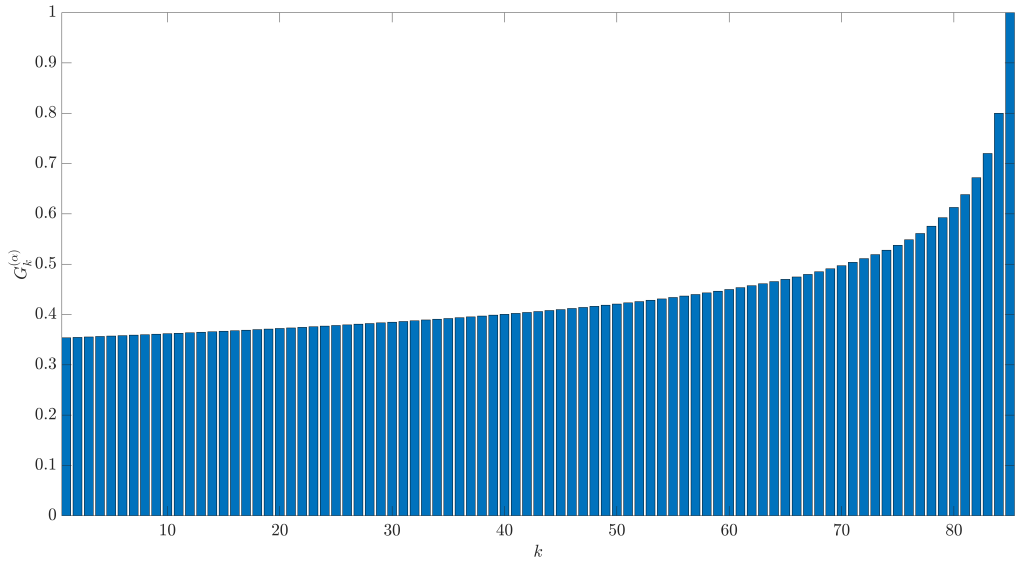

Figure 6. The weights G_k^{α} for the fractional logistic map (1). While the most recent iterations have the biggest impact on the next elements of the map, the memory horizon does reach the initial condition.

The proposed solution to this non-trivial question is based on the H-rank algorithm. However, the starting point of the sequence used to construct the Hankel matrix is now set not to the initial condition x_0, but to the iteration number where the control impulse is used. The pattern of H-ranks becomes the integral part of the proposed control scheme.

Initially, one needs to set the threshold δ and find m such that condition (7) holds true (after the initial transient leading to the finite-time stabilization of the unstable orbit). Then, the control impulse must bring the trajectory to a point $x_m = \widetilde{x}$, where $\widetilde{x}$ is set to the center of a yellow horizontal band in the pattern of H-ranks. The proposed control scheme for finite-time stabilization of the fractional difference logistic map is illustrated in Figure 7.

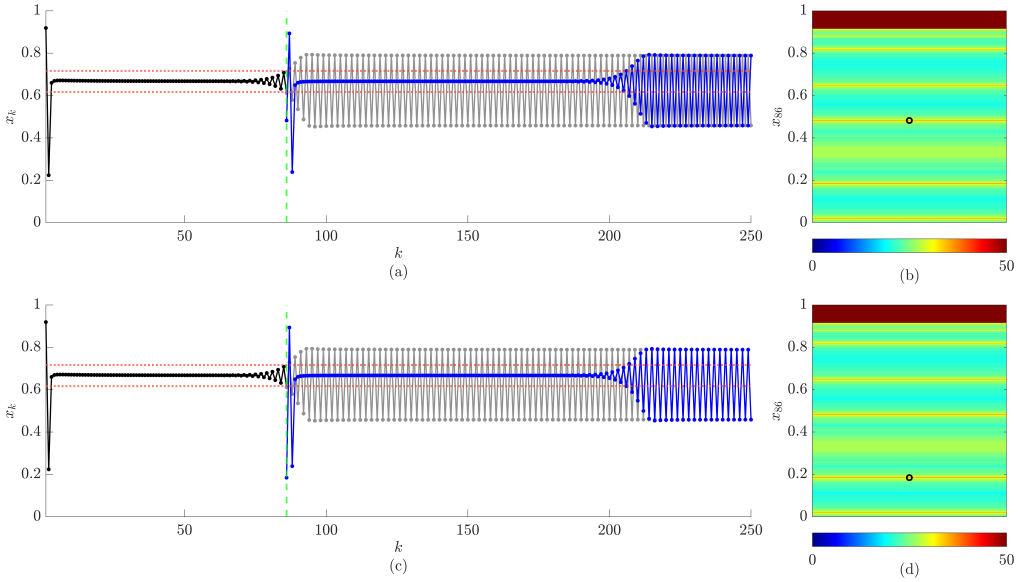

Figure 7. A single control impulse can stabilize the unstable orbit of the fractional difference logistic map for a finite time. The parameters of the model are set to: $\alpha = 0.8$; $a = 3$; $\delta = 0.05$. Red horizontal dotted lines denote the tolerance corridor around the unstable period-1 orbit: $x^* \pm \delta$. Black lines represent the trajectories of the fractional difference logistic map before stabilization impulse. Grey solid lines show how the trajectory would evolve if the control is not applied. Vertical green dashed lines denote the iteration number where the control impulse is applied. Blue lines represent trajectories after the stabilization impulse. Parts (**b**,**d**) depict the patterns of H-ranks computed time-forward starting from the stabilization moment. The black circles in (**b**,**d**) show the position of the map trajectory after the control impulse. Note that the unstable period-1 is stabilized in both panels (**a**,**c**). However, the transient processes are different right after the control impulse.

Note that the patterns of H-ranks in Figure 7 parts (b) and (d) are identical (except the markers showing the coordinates of the trajectory right after the control impulse). And though the unstable period-1 orbit is stabilized in both Figure 7 panels (a) and (b), the transient processes right after the control impulse are different. It is interesting to note that the complexity of the short transient processes after the control impulse depends on the chosen band in the pattern of the H-ranks (Figure 7). This is an interesting effect which could be exploited for the minimization of transient processes after the control impulse.

The proper selection of $\widetilde{x}$ is a key to this control scheme. As demonstrated in Figure 8a,b, the selection of $\widetilde{x}$ in the wide dark red band of highest possible H-ranks results in a divergent trajectory. Note that this fact does not contradict the boundedness of (1), since this divergence can only occur after the control impulse. Control impulses alter the memory of the map, making it possible for the divergence to occur.

A less extreme violation of the boundedness of (1) can be observed in Figure 8c,d: the selection of $\widetilde{x}$ close to the wide dark red band of H-ranks results in negative values of the fractional difference logistic map. However, in this case divergence does not occur as the trajectory later remains within $(0, 1)$. Of course, the unstable period-1 orbit is not stabilized then.

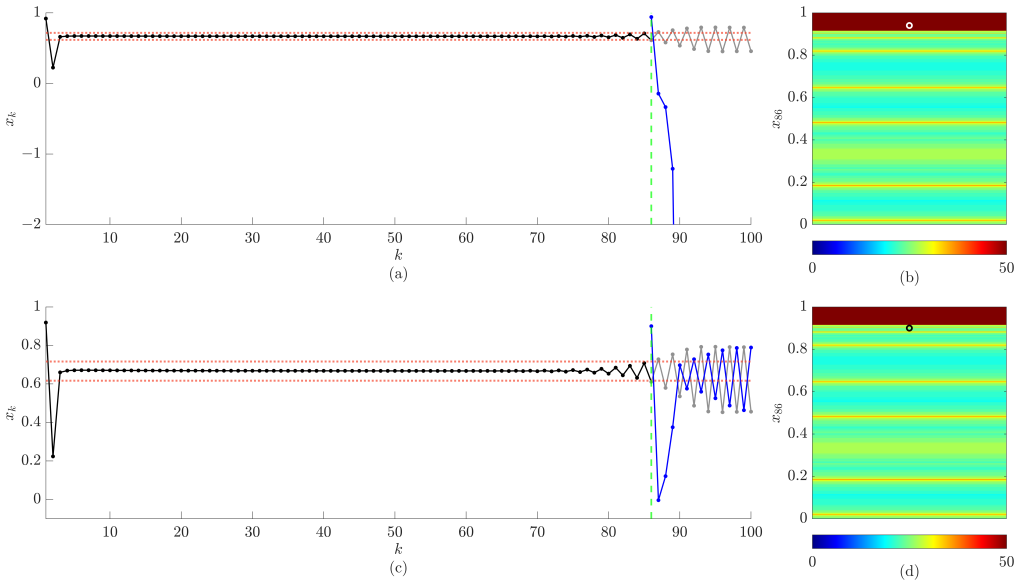

Figure 8. A proper selection of the control impulse is a key to the proposed scheme. Violation of the boundedness of the fractional logistic map with parameters $\alpha = 0.8$, $a = 3$, $\delta = 0.05$ is observed in panels (**a**,**c**). In (**a**,**c**), red dotted lines represent $x^* \pm \delta$; black lines represent the trajectories of the fractional logistic map before the impulse; gray solid lines show how the black lines would continue if the control impulse is not applied; blue lines represent trajectories after the stabilization impulse; the green dashed line represents the iteration at which the impulse is applied. Parts (**b**,**d**) depict the H-ranks computed time-forward starting from the stabilization impulse in (**a**,**c**), respectively. The white circle in (**b**) shows the trajectory after performing the stabilization impulse in (**a**); the black circle in (**d**) shows the trajectory after performing the stabilization impulse in (**d**). Note that the blue line in (**c**) dips below zero before asymptotically converging to the asymptotically stable period-2 orbit.

6. The Proposed Scheme Based on Multiple Control Impulses

It has been shown in the previous section that the proposed scheme based on a single control impulse does stabilize the unstable period-1 orbit of the fractional logistic map for a significant number of iterations. The same stabilization strategy can be used repeatedly (right after the stabilized trajectory no longer satisfies condition (7)). The described algorithm allows for indefinite stabilization of the unstable orbits of the fractional logistic map, with short bursts of transient processes after the application of the control impulse, as shown in Figure 9.

Note that the the patterns of H-ranks are different for each stabilization step (Figure 9b–d), which means a fixed coordinate $\widetilde{x}$ that can be used in every stabilization step does not exist. Instead, the patterns of H-ranks must be recomputed and the coordinate $\widetilde{x}$ must be chosen for each particular iteration. This property is not unexpected due to the non-locality of the fractional difference logistic map (1). The memory of the map is different at each stabilization point, which impacts (albeit sometimes imperceptibly) the pattern of H-ranks.

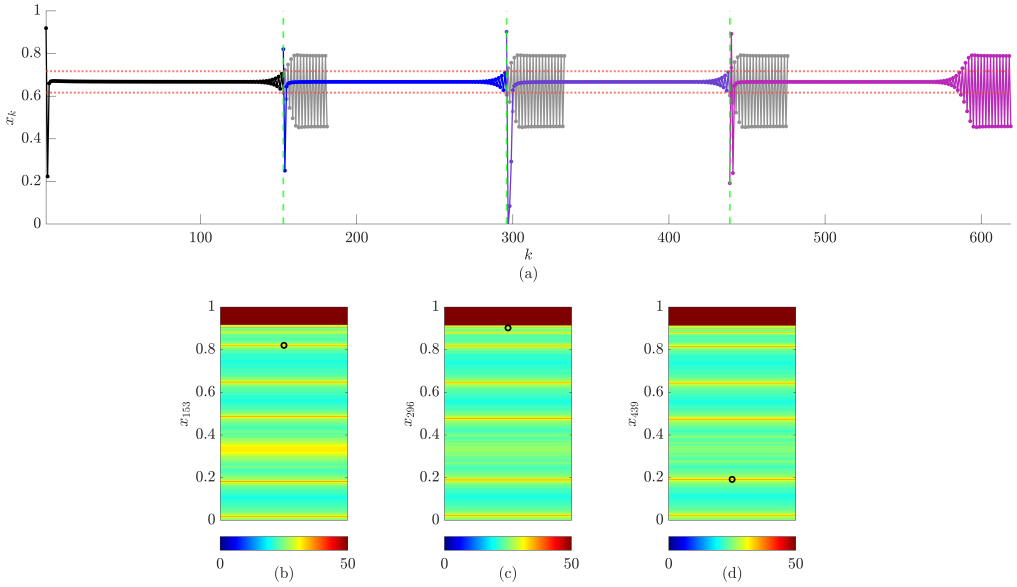

Figure 9. Realization of the proposed control scheme for the fractional difference logistic map at $\alpha = 0.8$, $a = 3$, $\delta = 0.05$ in part (**a**). Blue and purple lines denote stabilized trajectories; the pink line shows the trajectory asymptotically converging to the asymptotically stable period-2 orbit. Parts (**b**–**d**) depict the H-ranks computed time-forward starting from the first, second and third stabilization moments, respectively; black circles show the position of the map trajectories after respective control impulses.

7. Concluding Remarks

An impulse control scheme for the stabilization of unstable period-1 orbits of the fractional difference logistic map is proposed in this paper. The proposed impulse control scheme involves a perturbation of the system such that it remains in a small, 2δ-width band centered around the unstable period-1 orbit. Unlike feedback control schemes, the proposed impulse-based algorithm does not need to modify the logistic map and can be realized without error functions.

The concept of the H-rank of a sequence is the key to constructing this control scheme. It provides a simple yet efficient way to measure a signal's complexity and allows for the detection of temporarily asymptotically stable pseudo-manifolds of non-asymptotic convergence to unstable orbits. Numerical experiments with the fractional difference logistic demonstrate the efficiency and viability of this approach, although the potential use of this scheme is not limited to neither the analyzed model, nor the order of the unstable orbit. While only one value of the fractionality parameter $\alpha = 0.8$ is considered, the control scheme is not limited by this selection and is viable for any $0 < \alpha < 1$. A study on the impact of the value of parameter α on control scheme properties such as stabilization duration and transient processes, as well as the adaptation and refinement of the proposed H-rank-based impulse control scheme for other (not necessarily discrete) systems remains an objective of future research.

Author Contributions: Conceptualization, E.U., I.T., T.T. and M.R.; methodology, E.U., I.T., T.T. and M.R.; software, E.U.; validation, E.U.; formal analysis, I.T., T.T. and M.R.; investigation, E.U., I.T., T.T. and M.R.; writing—original draft preparation, E.U. and I.T. and T.T.; writing—review and editing, E.U., I.T., T.T. and M.R.; visualization, E.U.; supervision, M.R. All authors have read and agreed to the published version of the manuscript.

Funding: This research received no external funding

Conflicts of Interest: The authors declare no conflicts of interest.

References

1. Galor, O. *Discrete Dynamical Systems*; Springer Science & Business Media: Berlin/Heidelberg, Germany, 2007.
2. Smith, H.L.; Thieme, H.R. *Dynamical Systems and Population Persistence*; American Mathematical Soc.: Providence, RI, USA, 2011; Volume 118.
3. Hasegawa, Y. *Control Problems of Discrete-Time Dynamical Systems*; Springer: Berlin/Heidelberg, Germany, 2013; Volume 447.
4. Yang, X.; Deng, W.; Yao, J. Neural network based output feedback control for DC motors with asymptotic stability. *Mech. Syst. Signal Process.* **2022**, *164*, 108288. [CrossRef]
5. Vinoth, S.; Sivasamy, R.; Sathiyanathan, K.; Unyong, B.; Vadivel, R.; Gunasekaran, N. A novel discrete-time Leslie–Gower model with the impact of Allee effect in predator population. *Complexity* **2022**, *2022*, 6931354. [CrossRef]
6. Zheng, Y.; Yu, J. Stabilization of multi-rotation unstable periodic orbits through dynamic extended delayed feedback control. *Chaos Solitons Fractals* **2022**, *161*, 112362. [CrossRef]
7. Rodríguez-Núñez, J.M.; de León, A.; Molinar-Tabares, M.E.; Flores-Acosta, M.; Castillo, S. Computational chaos control based on small perturbations for complex spectra simulation. *Simulation* **2022**, *98*, 835–846. [CrossRef]
8. Hulka, T.; Matousek, R.; Lozi, R.P. Stabilization of Higher Periodic Orbits of Chaotic maps using Permutation-selective Objective Function. In Proceedings of the 2022 IEEE Workshop on Complexity in Engineering (COMPENG), IEEE, Florence, Italy, 18–20 July 2022; pp. 1–5.
9. Bramburger, J.J.; Kutz, J.N.; Brunton, S.L. Data-driven stabilization of periodic orbits. *IEEE Access* **2021**, *9*, 43504–43521. [CrossRef]
10. Weng, Y.; Zhang, Q.; Cao, J.; Yan, H.; Qi, W.; Cheng, J. Finite-time model-free adaptive control for discrete-time nonlinear systems. *IEEE Trans. Circuits Syst. II Express Briefs* **2023** . [CrossRef]
11. Edelman, M. Maps with power-law memory: Direct introduction and Eulerian numbers, fractional maps, and fractional difference maps. *Handb. Fract. Calc. Appl.* **2019**, *2*, 47–63.
12. Chen, L.; Yin, H.; Yuan, L.; Machado, J.T.; Wu, R.; Alam, Z. Double color image encryption based on fractional order discrete improved Henon map and Rubik's cube transform. *Signal Process. Image Commun.* **2021**, *97*, 116363. [CrossRef]
13. Zhu, L.; Jiang, D.; Ni, J.; Wang, X.; Rong, X.; Ahmad, M.; Chen, Y. A stable meaningful image encryption scheme using the newly-designed 2D discrete fractional-order chaotic map and Bayesian compressive sensing. *Signal Process.* **2022**, *195*, 108489. [CrossRef]
14. Liu, Z.; Xia, T.; Wang, T. Dynamic analysis of fractional-order six-order discrete chaotic mapping and its application in information security. *Optik* **2023**, *272*, 170356. [CrossRef]
15. Coll, C.; Herrero, A.; Ginestar, D.; S'anchez, E. The discrete fractional order difference applied to an epidemic model with indirect transmission. *Appl. Math. Model.* **2022**, *103*, 636–648. [CrossRef]
16. Abbes, A.; Ouannas, A.; Shawagfeh, N.; Grassi, G. The effect of the Caputo fractional difference operator on a new discrete COVID-19 model. *Results Phys.* **2022**, *39*, 105797. [CrossRef]
17. Chu, Y.M.; Bekiros, S.; Zambrano-Serrano, E.; Orozco-L'opez, O.; Lahmiri, S.; Jahanshahi, H.; Aly, A.A. Artificial macro-economics: A chaotic discrete-time fractional-order laboratory model. *Chaos Solitons Fractals* **2021**, *145*, 110776. [CrossRef]
18. Peng, Y.; Liu, J.; He, S.; Sun, K. Discrete fracmemristor-based chaotic map by Grunwald–Letnikov difference and its circuit implementation. *Chaos Solitons Fractals* **2023**, *171*, 113429. [CrossRef]
19. Edelman, M.; Jacobi, R. Power-Law Memory in Living Species and the Distribution of Lifespans. In Proceedings of the APS March Meeting Abstracts, Virtual, 15–19 March 2021; Volume 2021, p. L14–003 .
20. Zambrano-Serrano, E.; Bekiros, S.; Platas-Garza, M.A.; Posadas-Castillo, C.; Agarwal, P.; Jahanshahi, H.; Aly, A.A. On chaos and projective synchronization of a fractional difference map with no equilibria using a fuzzy-based state feedback control. *Phys. Stat. Mech. Its Appl.* **2021**, *578*, 126100. [CrossRef]
21. Lu, Q.; Zhu, Y.; Li, B. Necessary optimality conditions of fractional-order discrete uncertain optimal control problems. *Eur. J. Control.* **2023**, *69*, 100723. [CrossRef]
22. Yao, Y.; Wu, L.B. Backstepping control for fractional discrete-time systems. *Appl. Math. Comput.* **2022**, *434*, 127450. [CrossRef]
23. Shahamatkhah, E.; Tabatabaei, M. Containment control of linear discrete-time fractional-order multi-agent systems with time-delays. *Neurocomputing* **2020**, *385*, 42–47. [CrossRef]
24. Edelman, M. Universal fractional map and cascade of bifurcations type attractors. *Chaos Interdiscip. J. Nonlinear Sci.* **2013**, *23*, 033127. [CrossRef]
25. Edelman, M. Fractional maps and fractional attractors. Part II: Fractional difference caputo α-families of maps. *Discontinuity Nonlinearity Complex.* **2015**, *4*, 391–402. [CrossRef]
26. Kaslik, E.; Sivasundaram, S. Non-existence of periodic solutions in fractional-order dynamical systems and a remarkable difference between integer and fractional-order derivatives of periodic functions. *Nonlinear Anal. Real World Appl.* **2012**, *13*, 1489–1497. [CrossRef]
27. Diblík, J.; Fečkan, M.; Pospíšil, M. Nonexistence of periodic solutions and S-asymptotically periodic solutions in fractional difference equations. *Appl. Math. Comput.* **2015**, *257*, 230–240. [CrossRef]
28. Franklin, G.F.; Powell, J.D.; Emami-Naeini, A.; Powell, J.D. *Feedback Control of Dynamic Systems*; Prentice Hall: Upper Saddle River, NJ, USA, 2002; Volume 4.
29. Piunovskiy, A.; Plakhov, A.; Torres, D.F.; Zhang, Y. Optimal impulse control of dynamical systems. *Siam J. Control. Optim.* **2019**, *57*, 2720–2752. [CrossRef]

30. Lu, G.; Landauskas, M.; Ragulskis, M. Control of divergence in an extended invertible logistic map. *Int. J. Bifurc. Chaos* **2018**, *28*, 1850129. [CrossRef]
31. Landauskas, M.; Ragulskis, M. A pseudo-stable structure in a completely invertible bouncer system. *Nonlinear Dyn.* **2014**, *78*, 1629–1643. [CrossRef]
32. Navickas, Z.; Ragulskis, M.; Karaliene, D.; Telksnys, T. Weak and strong orders of linear recurring sequences. *Comput. Appl. Math.* **2018**, *37*, 3539–3561. [CrossRef]
33. Petkevičiūtė-Gerlach, D.; Timofejeva, I.; Ragulskis, M. Clocking convergence of the fractional difference logistic map. *Nonlinear Dyn.* **2020**, *100*, 3925–3935. [CrossRef]
34. Kurakin, V.; Kuzmin, A.; Mikhalev, A.; Nechaev, A. Linear recurring sequences over rings and modules. *J. Math. Sci.* **1995**, *76*, 2793–2915. [CrossRef]
35. Bisgard, J. *Analysis and Linear Algebra: The Singular Value Decomposition and Applications*; American Mathematical Soc.: Providence, RI, USA, 2020; Volume 94.
36. May, R.M. Simple mathematical models with very complicated dynamics. *Nature* **1976**, *261*, 459–467. [CrossRef]
37. Edelman, M. On stability of fixed points and chaos in fractional systems. *Chaos Interdiscip. J. Nonlinear Sci.* **2018**, *28*, 023112. [CrossRef]
38. Edelman, M. Evolution of systems with power-law memory: Do we have to die?(Dedicated to the Memory of Valentin Afraimovich). *Demogr. Popul. Health Aging Health Expend.* **2020**, *50*, 65–85.
39. Edelman, M. Stability of fixed points in generalized fractional maps of the orders $0< \alpha< 1$. *Nonlinear Dyn.* **2023**, *111*, 10247–10254.